Observabilty-Aware Trajectories for Geometric and Inertial Self-Calibration

Christoph Böhm[1], Guanrui Li[2], Giuseppe Loianno[2], and Stephan Weiss[1]

***Abstract*— In this paper, we apply an observability-aware trajectory generation method to the estimation of geometric and inertial parameters of an Unmanned Aerial System (UAS). These parameters are critical for reliable control and agile maneuvers, especially in the context of reconfiguration of the aerial vehicles during manipulation or transportation tasks. An extended observability analysis provides detailed insights on the observable and inter-state dependencies. We employ the observability-aware motion generation approach considering full system dynamics and self-calibration parameters. Improvements in the absolute error of ${}_B\mathbf{r}_{BP}$ estimates of up to 46.8% and decreases in uncertainty of up to 87% are achievable with this approach. Experiments with an autonomous quadrotor platform validate the approach.**

I. Introduction and Related Work

UAS (Unmanned Aerial Systems) as highly agile platforms push for robust, stable, and accurate state estimation and self-awareness for autonomous safe mission execution. Most applications combine different sensors to improve accuracy and allow redundancy of at least the control states (current position, velocity, and attitude). More sophisticated approaches (e.g. [2], [3], [4]), further include system calibration states to account for the on-line estimation of extrinsic sensor misalignment and intrinsic biases. This improves the accuracy of the control states [5] and allows for the health monitoring of sensors (e.g. misalignment after collision) and their signals (e.g. magnetic distortions). We focus on the so-called self-calibration capability and the extension with states for geometric and inertial properties of the UAS. Such properties are mass, the center of mass, moment of inertia, and extrinsic misalignment between the system's body frame, the IMU, and exteroceptive sensors (e.g. [1], [6], [7], [8]). Estimating these on-line enables the system to adjust not only to varying payloads or mechanical modifications during transportation or manipulation tasks [1], [9], [10], but also to other physical changes due to exogenous factors, and failures during the mission. This renders the UAS highly versatile and adjustable for different missions over a long duration without human intervention for system re-calibration. In particular, adding inertial properties to the estimation process via rotor speeds as system input in the UAS model, even IMU failures can be detected and compensated. Adding a multitude of states to a system asks for a thorough observability analysis (e.g. through [11]) to ensure proper state estimation at all times. As shown in [12], [13], not only the sensor quality plays an important role for the state estimation performance but also, and statistically probably more important, the generated system input (i.e. informative robot trajectories). It is vital to generate trajectories both enabling *well* observable states and avoiding unobservable modes. To achieve that, we make use of the non-linear observability analysis, [14] for identifying continuous symmetries and jointly observable states in the system, and [15] for the observability-aware optimization metric. The observability-aware optimization metric is an extension of the previously introduced idea in [16] of using the observability Gramian as measure of the quality of observabiltiy of a system. With that in mind, this paper focuses on the application of the observability-aware motion generation on a geometric and inertial properties based estimation framework [1]. It also demonstrates the need and effectiveness of well-chosen trajectories for fast and accurate state convergence. We present the following contributions: The extension of the quality of observability metric E^{2}LOG [12] to include geometric and inertial system properties through the inclusion of extended differentially flat trajectory properties. A detailed observability analysis of the unobservable, jointly observable, and fully observable states of a GNSS sensor configuration. The demonstration of the beneficial effect (absolute error reduction of up to 178% and a decrease in uncertainty of up to 87%) of E^{2}LOG optimized trajectories comparing our approach to the state of the art and random trajectories on the real system.

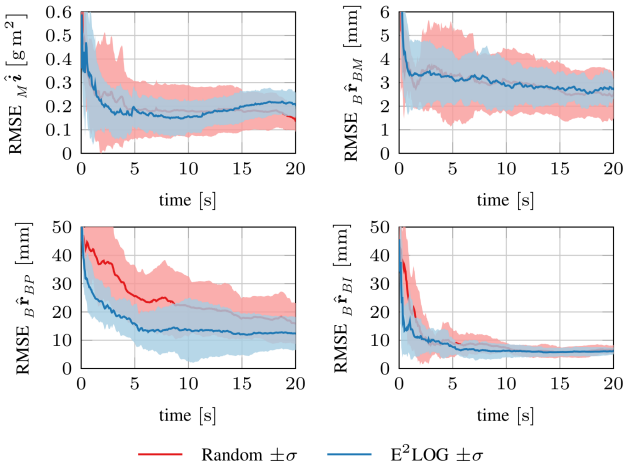

Fig. 1. Euclidean distance (or RMSE) convergence of EKF calibration state estimates compared to ground truth [1] for 20s random (red) and 20s optimized trajectories (blue). Curves show averages of the estimates with 1σ illustrating the variation in estimation accuracy over different trails.

[1] Christoph Böhm and Stephan Weiss are with the Institute of Smart System Technologies, Alpen-Adria-Universität Klagenfurt, Klagenfurt 9020, Austria. email: {christoph.boehm, stephan.weiss}@ieee.org

[2] Guanrui Li and Giuseppe Loianno are with the New York University, Tandon School of Engineering, Brooklyn, NY 11201, USA. email: {gl1871, loiannog}@nyu.edu

TABLE I. Visual overview of the observability analysis for the system setup described in Sec. II and [1].

Available Measurements	state vector dimension	observable dimension	${}_W\mathbf{r}_{WM}$	${}_W\mathbf{v}_{WM}$	$\mathbf{q}_{WM}$	${}_M\boldsymbol{\omega}_{WM}$	m	${}_M\boldsymbol{i}$	${}_B\mathbf{r}_{BM}$	${}_B\mathbf{r}_{BP}$	${}_B^{}\mathbf{r}_{BI}$ $[x, y]$	$\mathbf{b}_a$	$\mathbf{b}_\omega$
IMU only	18	17	u	u	u	ok	J1	ok	ok	u	ok	xy:ok z:J1	ok
GNSS only	23	22	ok	ok	ok	ok	ok	ok	xy:ok z:J2	xy:ok z:J2	u	u	u
Pose only	23	22	ok	ok	ok	ok	ok	ok	xy:ok z:J3	xy:ok z:J3	u	u	u
IMU & GNSS	31	31	ok	ok	ok	ok	ok	ok	ok	ok	ok	ok	ok
IMU & Pose	31	31	ok	ok	ok	ok	ok	ok	ok	ok	ok	ok	ok

II. Observability-Aware Trajectory Generation

The system model from Wuest et al. [1] is the starting point of our analysis and optimization. It assumes additive Gaussian noise in the process model $\mathbf{f}(\mathbf{x}, \mathbf{u})$ and measurement models $\mathbf{h}(\mathbf{x}, \mathbf{u})$ for the design of the EKF.

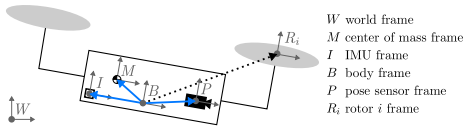

Fig. 2. Overview of the coordinate frames [1].

Following the representation in Fig. 2, we consider a fixed world frame W, the center of mass frame M, and the body-fixed frame B. A time-dependent state vector $\mathbf{x}_t$ contains all control states: position of M ${}_W\mathbf{r}_{WM}$, velocity of M ${}_W\mathbf{v}_{WM}$, orientation of M $\mathbf{q}_{WM}$, and angular velocity ${}_M\boldsymbol{\omega}_{WM}$ with respect to. W. We further specify a time-independent state vector $\mathbf{x}_c$. This state vector contains geometric and inertial parameters of the UAS: mass m, the moments of inertia ${}_M\boldsymbol{i}$, and the position of the center of mass ${}_B\mathbf{r}_{BM}$ with respect to B as well as self-calibration parameters of the sensors in use. An on-board IMU in the frame I measures linear acceleration and angular velocity. The VIO based pose sensor measures the position and orientation of the frame P with respect to W. Calibration states of the IMU and the pose sensor are their position on the UAS ${}_B\mathbf{r}_{BI}$, and ${}_B\mathbf{r}_{BP}$ respectively. The authors refer to [1] for a more detailed study.

A. Observability Analysis

A system is fully observable if the rank of the observability matrix $\mathcal{O}$ is equal to the size of the state vector. The observability matrix $\mathcal{O}$ of a non-linear system is composed of stacked gradients of Lie derivatives ∇L_i^h, as shown in [11]. Lie derivatives, therefore, are based on the measurement model $\mathbf{h}(\mathbf{x}, \mathbf{u})$ and zero-noise assumption, as suggested by [2].

$$L_0^h = \mathbf{h}(\mathbf{x}, \mathbf{u}) \quad L_{i+1}^h = \frac{\partial L_i^h}{\partial \mathbf{x}} \mathbf{f}(\mathbf{x}, \mathbf{u}) \tag{1}$$

Note that we did a variable substitution u_i^* for the squared rotor speeds as system inputs to enable the control-affine form.The null space of $\mathcal{O}$ and its spanning dimensions show unobservable and jointly observable states [14]. As entries depend on the current state values and control inputs, one can infer that the choice of trajectory impacts the quality of observability.

B. Discussion of Observability

We conducted additional observability analyses with this method to complement the work of [1]. This paper adds the study of global navigation satellite system (GNSS) measurements in isolation as well as combined with IMU information. GNSS measurements only provide position information, and it shows that the attitude information of the pose measurements yields redundant information. Position measurements and inertial readings already render the system of [1] fully observable. Tab. I shows a complete overview.

1) Measurements from GNSS: Having only position measurements available and no IMU measurements renders the calibration states of the IMU ${}_B\mathbf{r}_{BI}$, $\mathbf{b}_a$, and $\mathbf{b}_\omega$ unobservable. With the trajectory states $\mathbf{x}_t$, the overall state vector consists of 23 elements. The corresponding observability matrix $\mathcal{O}$ shows a rank deficiency of 1, caused by r_{BP_z} being jointly observable with r_{BM_z}. The position sensor's placement on our UAS allows the assumption $r_{BP_z} = 0$ to make the system fully observable. As one can see, additional attitude information from a pose sensor adds no information. Hence, position measurements from the GNSS or pose sensor will be sufficient for this setup. On another note, the angular velocity ${}_M\boldsymbol{\omega}_{WM}$ is observable even without IMU measurements. The IMU only serves as an update if available and improves estimation quality.

2) Measurements from GNSS and IMU: This configuration represents the outdoor use cases of a UAS, which makes it an interesting configuration to study. Adding r_{BI_z} to the state vector results in a joint observability between r_{BI_z}, r_{BP_z}, and r_{BM_z}. On our system, r_{BI_z} aligns with the body frame B in the z-direction, and the assumption $r_{BI_z} = 0$ renders all three states observable. Furthermore, position measurements make m observable, which results in b_{a_z} being observable as well. The rank test shows a fully observable system and, therefore, position measurements are sufficient for the estimation. In other words, the estimator can infer the system's orientation based on system dynamics and the resulting change in position.

These insights are important and need to be considered in the optimization of individual states because unobservable states won't allow convergence during optimization.

C. Expanded Empirical Local Observability Gramian

A state is well observable if the system output changes significantly by slightly perturbing the state value [4], [15]. The Expanded Empirical Local Observability Gramian (E^2LOG), [12], uses this fact to generate estimator-implementation agnostic observability-aware trajectories for a variety of systems. Inspired by [12], we approximate the input-output

map of a system with the n-th order Taylor expansion at t_0. Through the Jacobian, we obtain the sensitivity of the output with respect to the control input and state change. This reflects the idea of (quality of) observability.

$$\frac{\partial}{\partial \mathbf{x}} \mathbf{h}_{t_0}(\mathbf{x}(t), \mathbf{u}(t)) = \sum_{i=0}^{n} \frac{\delta t^i}{i!} \nabla L_i^h. \tag{2}$$

This time, the Lie derivatives are based on the control-nonaffine form of the system dynamics. With that, over the time horizon T follows:

$$\widetilde{W}_{t_0,T}(\theta) = \int_0^T K_{\theta,t_0}(t_0+t)^\intercal K_{\theta,t_0}(t_0+t) dt, \tag{3}$$

$$K_{\theta,t_0}(t) = \frac{\partial}{\partial \mathbf{x}} h_{t_0}(\mathbf{x}_\theta(t), \mathbf{u}_\theta(t)), \tag{4}$$

where $\mathbf{x}_\theta(t)$ and $\mathbf{u}_\theta(t)$ represent the system states and control inputs respectively. Both derive from a trajectory using the differential flat properties of the system [17]. This mapping from the 3D UAS trajectory as piece-wise polynomial to $\mathbf{x}_\theta(t)$ and $\mathbf{u}_\theta(t)$ is key to the optimization procedure highlighted in the following section. We refer to [12] for a more thorough derivation of the Expanded Empirical Local Observability Gramian (E^{2}LOG) $\widetilde{W}_0(\theta)$. This gramian makes it possible to generate trajectories that improve the system's convergence and make states better observable in general. Multi-state optimizations with the E^{2}LOG require K to use nominal values of all states. This avoids small changes in one state resulting in output changes dominating over other state's contributions. Column scaling the states with their corresponding standard deviations does this normalization. We ran 30 different random trajectories in order to determine each state's standard deviation.

D. Non-Linear Optimization & Data Generation

Wuest et al. [1] show the potential of estimating geometric and inertial properties of a UAS. Their results also show sub-optimal state convergence behavior across the state vector. These issues mainly manifest in very slow convergence and/or imprecise estimates. One example for both issues is ${}_B\mathbf{r}_{BP}$ with a final error of more than 15% and 25% in x- and y-direction respectively. We will show, with ${}_B\mathbf{r}_{BP}$, that we can estimate geometric and inertial self-calibration parameters of a UAS *faster* and *more precise* using the optimization problem as follows [12]:

$$\begin{aligned} &\text{maximize} && \sigma_{\min}(\widetilde{W}_0(\theta)) \\ &\text{subject to} && \theta \text{ suitable for task} \\ &&& \theta \text{ dynamically feasible} \end{aligned} \tag{5}$$

In words, the cost function maximizes the sensitivity of the output with respect to the input and states in the dimension where this sensitivity is lowest. We implemented this process in MATLAB and initialize the optimization with randomly generated trajectories. Non-linear inequality constraints keep the optimization within within system and dynamic limits: A maximum angular velocity of $\pm 2\pi$, a maximum travel of $1\,\mathrm{m}$ in all directions, maximum and minimum rotor speeds of $16400\,\mathrm{rpm}$ and $5500\,\mathrm{rpm}$, and a maximum roll and pitch angle of $70°$. These constraints demand knowledge of the mapping from piece-wise polynomial trajectory to individual rotor speeds. Mellinger and Kumar [17] show how one can get body velocities and accelerations from a sequence of differential flat outputs consisting of 3-D positions and yaw angles. With knowledge about the setup, the allocation matrix mapping velocities and accelerations to rotor speeds can be derived. We extend the E^{2}LOG approach in [12] with this element. Generating one optimized trajectory in MATLAB took around 5h on a Intel®Core™ i7-7820HQ notebook, reflecting the higher problem complexity compared to [15].

III. Experimental Results

In this section, we present the experiments that have been performed in the ARPL lab at the New York University indoor testbed with a flying space of $7 \times 5 \times 4\mathrm{m}^3$. The UAS platform is a so-called quadrotor, and uses a Qualcomm®Snapdragon™ board for on-board computations. The ground truth values for each geometric and inertial parameter of the quadrotor can be found in [1]. Software components during the experiments are a position and attitude controller, and a visual-inertial odometry (VIO) based pose estimation algorithm running at $30\mathrm{Hz}$. The VIO uses a down-facing camera and an IMU at $250\mathrm{Hz}$. For more details on the localization and control approaches, the reader can refer to our recent work [18], which demonstrates agile flight maneuvers in indoor environments.

A. Evaluation Method

We take the EKF results from [1] as a baseline for our performance evaluation. To show the beneficial effects of observability-aware motions, we tested two types of trajectories with the UAS. The first trial of trajectories are random ones with close to the same constraints as the optimized ones. Intuition tells us that those will perform worse than or as good as Lissajous figures. Then, a trail with ${}_B\mathbf{r}_{BP}$ optimized trajectories will show the improvement in performance achievable. All trajectories have a $20\mathrm{s}$ duration. A sampling-based method optimizing the EKF's end covariance is not considered due to the significantly increased computational effort. Preiss et al. [12] show similar effects of the end covariance optimization to self-calibration states as E^{2}LOG, but with 18 times longer computation time. VIO-based pose and IMU measurements have been recorded with ROS and are processed in the implemented EKF framework. All following evaluations and plots use the average of the estimates $\hat{\square}$ and covariances $\sigma^2_{\square}$ from each trail.

B. Discussion of Results

First we discuss the influence on ${}_B\hat{\mathbf{r}}_{BP}$ because it has been a problematic state in [1]. The estimate of ${}_B\hat{\mathbf{r}}_{BP}$ showed an absolute error of $-7.32\mathrm{mm}$ in x-, $-4.90\mathrm{mm}$ in y-, and $-2.14\mathrm{mm}$ in z-direction respectively. The euclidean distance or root mean squared error (RMSE) at the end of the trajectory is $9.1\mathrm{mm}$. Random trajectories generate an

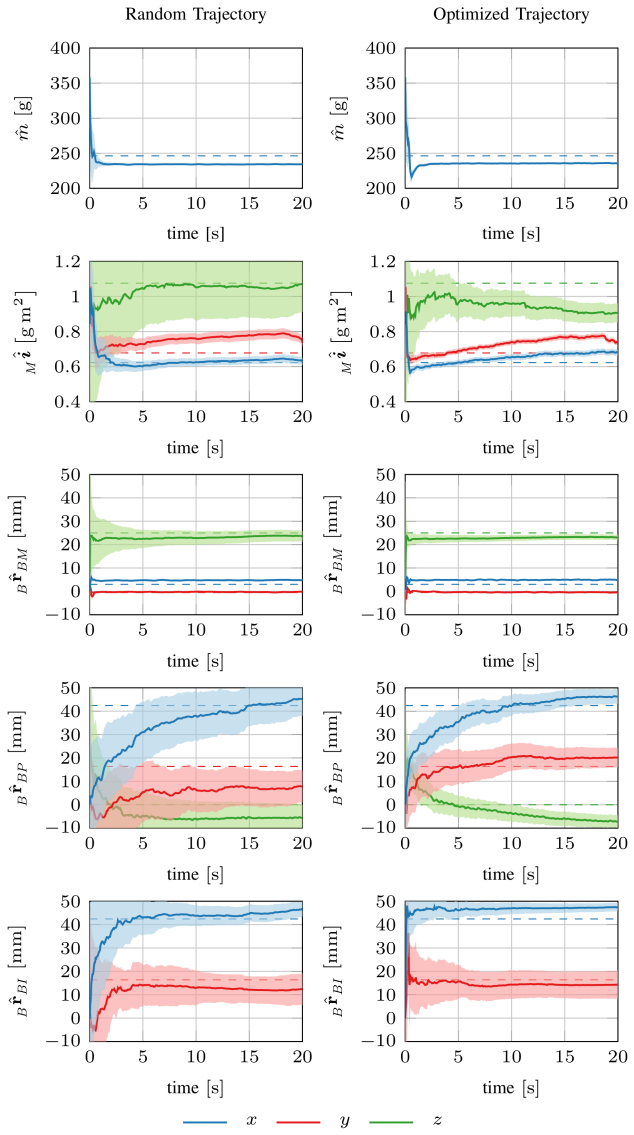

Fig. 3. Estimation result for the geometric and inertial parameters through the EKF based on 20s random trajectories (left) and 20s optimized trajectories (right). Curves show averages of the estimates and 1σ standard deviation as shaded ares over 10 test flights per trajectory type. The x variables are blue, y variables are red, and z variables are green.

average absolute error of 2.82mm in x-, -8.56mm in y-, and -5.62mm in z-direction with a RMSE of 15.8mm. This equals to a relative change in absolute error of -61.5%, $+74.7\%$, and $+162.6\%$ respectively. In contrast, ${}_B\hat{\mathbf{r}}_{BP}$ from the optimized trajectories shows on average an absolute error of 3.89mm in x-, 3.83mm in y-, and -7.18mm in z-direction with a RMSE of 12.1mm. The high error in z-direction is due to r_{BP_z} being zero and the resulting lack of excitement. One needs to take into account that the comparison against a single Lissajous figure might skew the results. A relative change in absolute error with respect to [1] of -46.8%, -21.8%, and $+235.5\%$ shows the improvements possible with optimized motions. Comparing this error with the random motion, we look at $+37.9\%$, -55.2%, and $+27,7\%$. Small offsets of the estimates can exist because of unmodeled effects (e.g. air drag or inaccurate thrust approximation). We optimized for the whole state ${}_B\mathbf{r}_{BP}$, meaning that individual components might have a higher absolute error (difference in region of 1mm) than other trails, but the RMSE shows an overall improvement. This can be seen in Fig. 1, where ${}_B\hat{\mathbf{r}}_{BP}$ converges at around 5 seconds to its value while the random trajectories struggles to converge this fast. Although we specifically ran the observability-aware optimization for ${}_B\mathbf{r}_{BP}$, the therefor generated motion is also beneficial for other states as seen in Fig. 3. On the other hand, states not optimized for and requiring different specific motion (as e.g. ${}_M\boldsymbol{i}_z$ requires large yaw motion for good convergence) naturally show lower performance. This causes the RMSE of ${}_M\hat{\boldsymbol{i}}$ to drift a bit off at the end. The IMU calibration state ${}_B\hat{\mathbf{r}}_{BI}$ improves as well with a relative changes of -26.0% and -48.2% compared to [1]. We see at least similar performance for the other states. The optimized trajectories are able to decrease the variance values of $\sigma^2_{{}_B\mathbf{r}_{BP}}$ by up to -82%, -63%, and -79% compared to random motions. A comparison with [1] is due to the lack of data not possible. Another good example is $\sigma^2_{{}_M\boldsymbol{i}}$ with up to -34%, -65%, and -87%. This shows the positive effect on the uncertainty of the EKF'S estimates.

IV. Conclusion

In this paper, we addressed the problem of observability-aware motion generation for complex state estimation. It presents an optimization approach for geometric and inertial self-calibration of UAS outperforming the current state of the art both in convergence accuracy and estimation precision. A thorough observability analysis revealed the joint observability of the different frames on the rigid body with respect to. their alignment in the z-direction (or one general direction if they had rotational offsets against each other). This supports the assumptions in [1] that the body and IMU frame have a known zero-z-offset, which renders the remaining states observable due to their joint inter-linkage. Furthermore, it showed that position measurements are sufficient to render the states fully observable. Therefore, attitude measures are redundant information. The optimization framework in [12] requires differential flat trajectories to optimize for selected states. For our problem set, we extended this differential flatness to individual rotor speeds of the UAS. Finally, the findings of the observability analysis and the extensions in the E^{2}LOG approach led to a framework achieving an improvement in the absolute error of ${}_B\mathbf{r}_{BP}$ of up to -46.8% compared to the state of the art. While maintaining the same or even lowering the convergence rate, a decrease in the EKF's variance of up to -87% is achievable. There is a clear motivation for using observability-aware motion generation for geometric and inertial self-calibration on UASs with these improvements. Future works will consider the ability to extend this framework to estimate properties of physically interconnected aerial systems. We would also like to investigate the performances for a large repertoire of grasping maneuvers, where the system needs to reconfigure and re-estimate in real-time the geometric and inertial parameters based on the payload.

REFERENCES

[1] V. Wuest, V. Kumar, and G. Loianno, "Online Estimation of Geometric and inertia parameters for multirotor aerial vehicles," in *IEEE International Conference on Robotics and Automation (ICRA)*, May 2019.

[2] J. Kelly and G. S. Sukhatme, "Visual-Inertial Sensor Fusion: Localization, Mapping and Sensor-to-Sensor Self-Calibration," *The International Journal of Robotics Research (IJRR)*, vol. 30, no. 1, pp. 56–79, 2011.

[3] S. Weiss and R. Siegwart, "Real-Time Metric State Estimation for Modular Vision-Inertial Systems," in *2011 IEEE International Conference on Robotics and Automation (ICRA)*, May 2011, pp. 4531–4537.

[4] S. Weiss, "Vision Based Navigation for Micro Helicopters," Ph.D. dissertation, ETH Zurich, 2012. [Online]. Available: https://www.research-collection.ethz.ch/bitstream/handle/20.500.11850/52698/eth-5889-02.pdf

[5] M. W. Achtelik, S. Lynen, M. Chli, and R. Siegwart, "Inversion Based Direct Position Control and Trajectory Following for Micro Aerial Vehicles," in *2013 IEEE/RSJ International Conference on Intelligent Robots and Systems (IROS)*, Nov 2013, pp. 2933–2939.

[6] M. Burri, M. Dätwiler, M. W. Achtelik, and R. Siegwart, "Robust State Estimation for Micro Aerial Vehicles Based on System Dynamics," in *2015 IEEE International Conference on Robotics and Automation (ICRA)*, May 2015, pp. 5278–5283.

[7] M. Burri, J. Nikolic, H. Oleynikova, M. W. Achtelik, and R. Siegwart, "Maximum Likelihood Parameter Identification for MAVs," in *2016 IEEE International Conference on Robotics and Automation (ICRA)*, May 2016, pp. 4297–4303.

[8] M. Burri, M. Bloesch, Z. Taylor, R. Siegwart, and J. Nieto, "A framework for maximum likelihood parameter identification applied on MAVs," *Journal of Field Robotics (JFR)*, vol. 35, no. 1, pp. 5–22, 2018.

[9] G. Loianno and V. Kumar, "Cooperative transportation using small quadrotors using monocular vision and inertial sensing," *IEEE Robotics and Automation Letters*, vol. 3, no. 2, pp. 680–687, April 2018.

[10] G. Loianno, V. Spurny, J. Thomas, T. Baca, D. Thakur, D. Hert, R. Penicka, T. Krajnik, A. Zhou, A. Cho, M. Saska, and V. Kumar, "Localization, grasping, and transportation of magnetic objects by a team of mavs in challenging desert-like environments," *IEEE Robotics and Automation Letters*, vol. 3, no. 3, pp. 1576–1583, July 2018.

[11] R. Hermann and A. Krener, "Nonlinear Controllability and Observability," *IEEE Transactions on Automatic Control (TAC)*, vol. 22, no. 5, pp. 728–740, October 1977.

[12] J. A. Preiss, K. Hausman, G. S. Sukhatme, and S. Weiss, "Simultaneous self-calibration and navigation using trajectory optimization," *The International Journal of Robotics Research (IJRR)*, vol. 37, no. 13-14, pp. 1573–1594, 2018.

[13] J. A. Preiss, K. Hausman, G. S. Sukhatme, and S. Weiss, "Trajectory Optimization for Self-Calibration and Navigation," in *Proceedings of Robotics: Science and Systems XIII (RSS)*, July 2017. [Online]. Available: http://www.roboticsproceedings.org/rss13/p54.pdf

[14] A. Martinelli, "Continuous Symmetries and Observability Properties in Autonomous Navigation," INRIA, Research Report RR-7049, 2010. [Online]. Available: https://hal.inria.fr/inria-00421233

[15] K. Hausman, J. Preiss, G. S. Sukhatme, and S. Weiss, "Observability-Aware Trajectory Optimization for Self-Calibration With Application to UAVs," *IEEE Robotics and Automation Letters (RA-L)*, vol. 2, no. 3, pp. 1770–1777, July 2017.

[16] A. J. Krener and K. Ide, "Measures of Unobservability," in *Proceedings of the 48h IEEE Conference on Decision and Control (CDC)*, Dec 2009, pp. 6401–6406.

[17] D. Mellinger and V. Kumar, "Minimum Snap Trajectory Generation and Control for Quadrotors," in *2011 IEEE International Conference on Robotics and Automation (ICRA)*, May 2011, pp. 2520–2525.

[18] G. Loianno, C. Brunner, G. McGrath, and V. Kumar, "Estimation, control, and planning for aggressive flight with a small quadrotor with a single camera and imu," *IEEE Robotics and Automation Letters*, vol. 2, no. 2, pp. 404–411, April 2017.